Spot size characterization of focused non-Gaussian X-ray laser beams

J. Chalupský,[1,2*] J. Krzywinski,[3] L. Juha,[1] V. Hájková,[1] J. Cihelka,[1] T. Burian,[1] L. Vyšín,[1] J. Gaudin,[4] A. Gleeson,[5] M. Jurek,[6] A. R. Khorsand,[7] D. Klinger,[6] H. Wabnitz,[9] R. Sobierajski,[6,8] M. Störmer,[10] K. Tiedtke,[9] and S. Toleikis[9]

[1]*Institute of Physics, Academy of Sciences of the Czech Republic, Na Slovance 2, 182 21 Prague 8, Czech Republic*
[2]*Czech Technical University in Prague, Brehova 7, 115 19 Praha 1, Czech Republic*
[3]*SLAC National Accelerator Laboratory, 2575 Sand Hill Road, Menlo Park, California 94025, USA*
[4]*European XFEL, Albert-Einstein-Ring 19, 22761 Hamburg, Germany*
[5]*STFC Daresbury Laboratory, Warrington, Cheshire, WA4 4AD, UK*
[6]*Institute of Physics, Polish Academy of Sciences, Al. Lotników 32/46, PL-02-668 Warsaw, Poland*
[7]*Radboud University Nijmegen, Heijendaalseweg 135, 6525 AJ Nijmegen, The Netherlands*
[8]*FOM-Institute for Plasma Physics Rijnhuizen, P.O. Box 1207, 3430 BE Nieuwegein, The Netherlands*
[9]*Deutsches Elektronen-Synchrotron DESY, Notkestrasse 85, 22607 Hamburg, Germany*
[10]*Helmholtz-Zentrum Geesthacht, Max-Planck-Strasse 1, 21502 Geesthacht, Germany*
**chal@fzu.cz*
www.fzu.cz

Abstract: We present a new technique for the characterization of non-Gaussian laser beams which cannot be described by an analytical formula. As a generalization of the beam spot area we apply and refine the definition of so called effective area (A_{eff}) [1] in order to avoid using the full-width at half maximum (FWHM) parameter which is inappropriate for non-Gaussian beams. Furthermore, we demonstrate a practical utilization of our technique for a femtosecond soft X-ray free-electron laser. The ablative imprints in poly(methyl methacrylate) - PMMA and amorphous carbon (a-C) are used to characterize the spatial beam profile and to determine the effective area. Two procedures of the effective area determination are presented in this work. An F-scan method, newly developed in this paper, appears to be a good candidate for the spatial beam diagnostics applicable to lasers of various kinds.

OCIS codes: (140.7240) Lasers and laser optics: UV, XUV, and X-ray lasers; (140.2600) Lasers and laser optics: Free electron lasers; (340.0340) X-ray optics; (120.0120) Instrumentation, measurement, and metrology.

References and links

1. ISO 11254–1:2000, "Laser and laser-related equipment - Determination of laser-induced damage threshold of optical surfaces - Part 1: 1-on-1 test,"
2. J. Chalupský, L. Juha, J. Kuba, J. Cihelka, V. Hájková, S. Koptyaev, J. Krása, A. Velyhan, M. Bergh, C. Caleman, J. Hajdu, R. M. Bionta, H. Chapman, S. P. Hau-Riege, R. A. London, M. Jurek, J. Krzywinski, R. Nietubyc, J. B. Pelka, R. Sobierajski, J. Meyer-Ter-Vehn, A. Tronnier, K. Sokolowski-Tinten, N. Stojanovic, K. Tiedtke, S. Toleikis, T. Tschentscher, H. Wabnitz, and U. Zastrau, "Characteristics of focused soft X-ray free-electron laser beam determined by ablation of organic molecular solids," Opt. Express **15**(10), 6036–6043 (2007).
3. S. Le Pape, Ph. Zeitoun, M. Idir, P. Dhez, J. J. Rocca, and M. François, "Electromagnetic-field distribution measurements in the soft x-ray range: full characterization of a soft x-ray laser beam," Phys. Rev. Lett. **88**(18), 183901 (2002).
4. M. Kirm, A. Andrejczuk, J. Krzywinski, and R. Sobierajski, "Influence of excitation density on luminescence decay in $Y_3Al_5O_{12}$:Ce and BaF_2 crystals excited by free electron laser radiation in VUV," Phys. Status Solidi, C Conf. Crit. Rev. **2**(1), 649–652 (2005).
5. A. J. Nelson, S. Toleikis, H. Chapman, S. Bajt, J. Krzywinski, J. Chalupsky, L. Juha, J. Cihelka, V. Hajkova, L. Vysin, T. Burian, M. Kozlova, R. R. Fäustlin, B. Nagler, S. M. Vinko, T. Whitcher, T. Dzelzainis, O. Renner, K. Saksl, A. R. Khorsand, P. A. Heimann, R. Sobierajski, D. Klinger, M. Jurek, J. Pelka, B. Iwan, J. Andreasson, N. Timneanu, M. Fajardo, J. S. Wark, D. Riley, T. Tschentscher, J. Hajdu, and R. W. Lee, "Soft x-ray free electron laser microfocus for exploring matter under extreme conditions," Opt. Express **17**(20), 18271–18278 (2009).

#136453 - $15.00 USD Received 14 Oct 2010; revised 3 Dec 2010; accepted 6 Dec 2010; published 17 Dec 2010

6. ISO 11146–1:2005, "Lasers and laser-related equipment - Test methods for laser beams widths, divergence angles and beam propagation ratios - Part 1: Stigmatic and simple astigmatic beams,"
7. ISO 11146–2:2005, "Lasers and laser-related equipment - Test methods for laser beam widths, divergence angles and beam propagation ratios - Part 2: General astigmatic beams,"
8. ISO 11146:1999, "Lasers and laser-related equipment - Test methods for laser beam parameters – Beam widths, divergence angle and beam propagation factor,"
9. K. Tiedtke, A. Azima, N. von Bargen, L. Bittner, S. Bonfigt, S. Düsterer, B. Faatz, U. Frühling, M. Gensch, Ch. Gerth, N. Guerassimova, U. Hahn, T. Hans, M. Hesse1, K. Honkavaar, U. Jastrow, P. Juranic, S. Kapitzki, B. Keitel, T. Kracht, M. Kuhlmann, W. B. Li, M. Martins, T. Núñez, E. Plönjes, H. Redlin, E. L. Saldin, E. A. Schneidmiller, J. R. Schneider, S. Schreiber, N. Stojanovic, F. Tavella, S. Toleikis, R. Treusch, H. Weigelt, M. Wellhöfer, H. Wabnitz, M. V. Yurkov, and J. Feldhaus, "The soft x-ray free-electron laser FLASH at DESY: beamlines, diagnostics and end-stations," N. J. Phys. **11**, 023029 (2009).
10. V. Ayvazyan, N. Baboi, I. Bohnet, R. Brinkmann, M. Castellano, P. Castro, L. Catani, S. Choroba, A. Cianchi, M. Dohlus, H. T. Edwards, B. Faatz, A. A. Fateev, J. Feldhaus, K. Flöttmann, A. Gamp, T. Garvey, H. Genz, Ch. Gerth, V. Gretchko, B. Grigoryan, U. Hahn, C. Hessler, K. Honkavaara, M. Hüning, R. Ischebeck, M. Jablonka, T. Kamps, M. Körfer, M. Krassilnikov, J. Krzywinski, M. Liepe, A. Liero, T. Limberg, H. Loos, M. Luong, C. Magne, J. Menzel, P. Michelato, M. Minty, U. C. Müller, D. Nölle, A. Novokhatski, C. Pagani, F. Peters, J. Pflüger, P. Piot, L. Plucinski, K. Rehlich, I. Reyzl, A. Richter, J. Rossbach, E. L. Saldin, W. Sandner, H. Schlarb, G. Schmidt, P. Schmüser, J. R. Schneider, E. A. Schneidmiller, H. J. Schreiber, S. Schreiber, D. Sertore, S. Setzer, S. Simrock, R. Sobierajski, B. Sonntag, B. Steeg, F. Stephan, K. P. Sytchev, K. Tiedtke, M. Tonutti, R. Treusch, D. Trines, D. Türke, V. Verzilov, R. Wanzenberg, T. Weiland, H. Weise, M. Wendt, I. Will, S. Wolff, K. Wittenburg, M. V. Yurkov, and K. Zapfe, "Generation of GW radiation pulses from a VUV free-electron laser operating in the femtosecond regime," Phys. Rev. Lett. **88**(10), 104802 (2002).
11. B. Nagler, U. Zastrau, R. Fäustlin, S. M. Vinko, T. Whitcher, A. J. Nelson, R. Sobierajski, J. Krzywinski, J. Chalupsky, E. Abreu, S. Bajt, T. Bornath, T. Burian, H. Chapman, J. Cihelka, T. Döppner, S. Düsterer, T. Dzelzainis, M. Fajardo, E. Förster, C. Fortmann, E. Galtier, S. H. Glenzer, S. Göde, G. Gregori, V. Hajkova, P. Heimann, L. Juha, M. Jurek, F. Y. Khattak, A. R. Khorsand, D. Klinger, M. Kozlova, T. Laarmann, H. J. Lee, R. W. Lee, K. H. Meiwes-Broer, P. Mercere, W. J. Murphy, A. Przystawik, R. Redmer, H. Reinholz, D. Riley, G. Röpke, F. Rosmej, K. Saksl, R. Schott, R. Thiele, J. Tiggesbäumker, S. Toleikis, T. Tschentscher, I. Uschmann, H. J. Vollmer, and J. S. Wark, "Turning solid aluminium transparent by intense soft X-ray photoionization," Nat. Phys. **5**(9), 693–696 (2009).
12. C. Bostedt, H. Thomas, M. Hoener, E. Eremina, T. Fennel, K.-H. Meiwes-Broer, H. Wabnitz, M. Kuhlmann, E. Plönjes, K. Tiedtke, R. Treusch, J. Feldhaus, A. R. de Castro, and T. Möller, "Multistep ionization of argon clusters in intense femtosecond extreme ultraviolet pulses," Phys. Rev. Lett. **100**(13), 133401 (2008).
13. T. W. J. Dzelzainis, J. Chalupsky, M. Fajardo, R. Fäustlin, P. A. Heimann, V. Hajkova, L. Juha, M. Jurek, F. Y. Khattak, M. Kozlova, J. Krzywinski, R. W. Lee, B. Nagler, A. J. Nelson, F. B. Rosmej, R. Sobierajski, S. Toleikis, T. Tschentscher, S. M. Vinko, J. S. Wark, T. Whitcher, and D. Riley, "Plasma emission spectroscopy of solids irradiated by intense XUV pulses from a free electron laser," High Energy Density Phys. **6**(1), 109–112 (2010).
14. P. Johnsson, A. Rouzée, W. Siu, Y. Huismans, F. Lépine, T. Marchenko, S. Düsterer, F. Tavella, N. Stojanovic, A. Azima, R. Treusch, M. F. Kling, and M. J. J. Vrakking, "Field-free molecular alignment probed by the free electron laser in Hamburg (FLASH)," J. Phys. B **42**(13), 134017 (2009).
15. A. Barty, R. Soufli, T. McCarville, S. L. Baker, M. J. Pivovaroff, P. Stefan, and R. Bionta, "Predicting the coherent X-ray wavefront focal properties at the Linac Coherent Light Source (LCLS) X-ray free electron laser," Opt. Express **17**(18), 15508–15519 (2009).
16. B. E. A. Saleh, and M. C. Teich, *Fundamentals of Photonics* (John Wiley & Sons, New York, 1991), Chap. 3.
17. A. E. Siegman, "How to (Maybe) Measure Laser Beam Quality," in *DPSS (Diode Pumped Solid State) Lasers: Applications and Issues*, M. Dowley, ed., Vol. **17** of OSA Trends in Optics and Photonics (Optical Society of America, 1998), pp. 184–199, paper MQ1. http://www.opticsinfobase.org/abstract.cfm?uri=DLAI-1998-MQ1
18. J. M. Liu, "Simple technique for measurements of pulsed Gaussian-beam spot sizes," Opt. Lett. **7**(5), 196–198 (1982).
19. http://henke.lbl.gov/optical_constants/
20. M. Richter, A. Gottwald, U. Kroth, A. A. Sorokin, S. V. Bobashev, L. A. Shmaenok, J. Feldhaus, C. Gerth, B. Steeg, K. Tiedtke, and R. Treusch, "Measurement of gigawatt radiation pulses from a vacuum and extreme ultraviolet free-electron laser," Appl. Phys. Lett. **83**(14), 2970–2972 (2003).

1. Introduction

Rapid development of short-wavelength lasers in recent years opened new areas in the field of the laser-matter interaction research. The optimization as well as the use of these new light sources in numerous experiments requires a careful characterization of their output parameters. In dealing with such ultra-intense beams at short wavelengths, new laser beam diagnostics have to be developed and an extensive research in this area is needed.

Up to now, a few methods have been reported for determination of the beam profile of soft X-ray lasers [2–4]. These tools are being frequently used for aligning the X-ray optics and improving the beam profile of short-wavelength lasers. However, it is difficult, and in most

#136453 - $15.00 USD Received 14 Oct 2010; revised 3 Dec 2010; accepted 6 Dec 2010; published 17 Dec 2010

cases it is almost not feasible to obtain a perfect Gaussian beam since in extreme ultraviolet (XUV), soft X-ray, and X-ray spectral regions the laser beam is often exhibiting severe imperfections in its wavefront. Such wavefront distortions can originate in the source itself; they are very typical of ASE (Amplified Spontaneous Emission) and/or SASE (Self-Amplified Spontaneous Emission) mechanisms of lasing. In addition, when dealing with coherent laser beams, the wavefront can be affected by imperfections in beamline optical elements.

In the soft X-ray and X-ray spectral domain, the coherent radiation reflecting from a mirror feels more sensitively the surface roughness (usually measured in fractions of the wavelength). Firstly, rough and imperfect mirror surfaces may introduce additional unwanted wavefront distortions into the beam hindering from the diffraction limited focusing. Secondly, the reflecting surface roughness leads also to some light to be scattered off the original laser beam direction. Therefore, precise and well polished optical surfaces are required. Besides the surface roughness limitations, the reflectivity of all routinely used optical materials is inherently dropping for shorter X-ray wavelengths, corresponding to photon energies above the K-edge of these materials (in the range of hundreds eV up to few keV). Hence, grazing incidence techniques and multi-layer coatings are used in order to partially compensate for the insufficient reflectance. These effects, resulting in energy density losses, are enhancing as the photon energy increases and are unavoidably setting limits on the reflective optics. Consequently, no additional flux losses are acceptable and, therefore, a huge emphasis is being placed on a perfect aberration-free mirror alignment [5]. Hence, good techniques of the beam visualization are indispensable for the alignment of the soft X-ray and X-ray focusing optics.

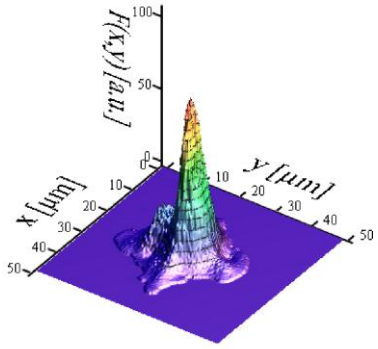

Fig. 1. A non-Gaussian beam profile of FLASH at 13.5 nm reconstructed from a non-thermal ablative imprint in PMMA.

There are several possibilities to assess the quality of the incident beam. The most important parameters of the transverse (lateral) irradiance distribution in a Gaussian beam (TEM_{00}) are those measuring the beam size as, for example, full-width at half maximum (FWHM), a diameter (2ρ) at 1/e of its maximum, a diameter at any other chosen level of the peak irradiance (arbitrary clip level), or diameters related to 2nd order statistical moments (4σ, root mean square) [6–8]. Their values are deterministically mutually related in this particular case. Subsequently, if the pulse energy E_{pulse} is known, the peak fluence can be expressed as $F_0 = E_{pulse}/\pi\rho^2$. However, the value of F_0 cannot be retrieved from the preceding formula in case of non-Gaussian (distorted, non-homogeneous) beams as, for example, the one illustrated in Fig. 1. This beam profile, measured at beamline BL2 [9] of the FLASH (Free-electron Laser in Hamburg) facility [10] tuned at 13.5 nm, clearly indicates a deviation from an ideal Gaussian beam preventing the standard spot size description by means of the FWHM, the 1/e, or the $1/e^2$ clip level. A method reported in [2] has been utilized to retrieve the beam profile in Fig. 1.

#136453 - $15.00 USD Received 14 Oct 2010; revised 3 Dec 2010; accepted 6 Dec 2010; published 17 Dec 2010

Finally, it is to be pointed out that a profound knowledge of the peak fluence F_0 or the peak irradiance is of high importance for many irradiance-dependent short-wavelength laser-matter interaction experiments, e.g., warm-dense matter experiments [5,11], ion and photon emission spectrometry [12,13], various pump-probe experiments [14] etc. Routinely used beam spot size definitions (FWHM, 2ρ) are to be regarded as an approach for non-Gaussian beams; therefore, a reliable formalism is needed for accurate spot size and peak fluence determination. In the following (section 2), we aim at the theory of the effective area which might be considered as a quantity of interest for non-Gaussian beam diagnostics. We compare the effective area with other well-known spot size definitions (FWHM, 1/e clip level, and diameters related to 2nd order statistical moments). Section 3 deals with our experimental methods and the results of measuring the focused non-Gaussian X-ray laser beam. Section 4 concludes the paper.

2. Theory

Non-Gaussian beams cannot be characterized by means of FWHM reliably; nevertheless, it is worth mentioning that the so called effective area A_{eff} [1] is still applicable. Let us first define a general spatial time-integrated fluence distribution of a propagating beam at any point (x,y,z) in the Cartesian coordinate system as:

$$F(x,y,z) = F_0(z)\, f(x,y,z). \tag{1}$$

Here, $F_0(z)$ is a z-dependent peak fluence and f(x,y,z) is a spatial beam profile. The z-coordinate denotes the direction of the beam propagation (optical axis) and the (x,y) plane corresponds to the transverse plane. For example in a Gaussian beam, the function $F_0(z)$ is represented by a Lorentzian curve forming a longitudinal envelope of transverse Gaussian profiles f(x,y,z). We can apply Eq. (1) to any beam propagating in the space since any beam must have a global transverse maximum (peak fluence) at a certain arbitrary z-position.

The existence of the global maximum $F_0(z)$ and the non-negativity of F(x,y,z) implies that the beam profile function fulfills $0 \le f(x,y,z) \le 1$ throughout the (x,y) plane at each z-position. In more details, we may state that for each z-position there exists at least one point in the (x,y) plane for which f(x,y,z) = 1. In an ideal Gaussian beam, the geometrical solution of this implicit equation represents a straight line overlapping the optical axis. In real beams, the maximum may move around the optical axis, and multiple maxima may appear; hence, the solution of this equation can be no longer described by a straight line.

In order to retrieve the beam profile function f(x,y,z), we normalize the fluence distribution F(x,y,z) at each z-position by so called uniform norm which is represented by $F_0(z)$. The spatial beam profile function f(x,y,z), therefore, still contains important information about the beam spot size since the surface integral throughout the (x,y) plane does not equal to the dimensionless unity. Let us first calculate the pulse energy E_{pulse} as a two-dimensional integral of F(x,y,z) over the x,y variables in the transverse direction:

$$E_{pulse} = F_0(z) \iint_{R^2} f(x,y,z)\, dxdy = F_0(z)\, A_{eff}(z) = const., \tag{2a}$$

featuring the effective caustic curve $A_{eff}(z)$, i.e., the effective area A_{eff} at an arbitrary z-position, as:

$$A_{eff}(z) = \frac{E_{pulse}}{F_0(z)} = \iint_{R^2} f(x,y,z)\, dxdy. \tag{2b}$$

The first equality in Eq. (2b) is representing the definition of the effective area in [1]. The effective area can be understood as a generalization of the beam spot area defined as the cross-section area at 1/e of the peak fluence. Applying Eq. (2b) to a circular Gaussian beam defined as $f(x,y,z) = \exp(-(x^2 + y^2)/\rho^2(z))$, we obtain $A_{eff}(z) = \pi\rho^2(z)$ which corresponds exactly to the beam spot area at 1/e of the peak fluence. Here, $\rho(z) = \rho_0(1 + z^2/z_0^2)^{1/2}$ denotes

#136453 - $15.00 USD Received 14 Oct 2010; revised 3 Dec 2010; accepted 6 Dec 2010; published 17 Dec 2010

the beam radius at an arbitrary z-position (ρ_0 - diffraction limited beam waist radius at 1/e of maximum; z_0 – Rayleigh range). This is, however, solely valid for Gaussian beams. It is reasonable to use the effective area for non-Gaussian beams since it is applicable to any beam profile and it is fully mathematically correct. On the contrary to the beam RMS (root mean square or 2nd order statistical moments), routinely used in synchrotron communities, the effective area relates directly (see Eq. (2a) or Eq. (2b)) the peak fluence and the pulse energy as $F_0(z) = E_{pulse}/A_{eff}(z)$. As no approximations are used in the definition of A_{eff}, it can be used as a fundamental parameter to which all the other spot size definitions refer when an exact knowledge of the peak fluence is needed. In the following, we compare the most utilized spot size definitions with the effective area.

The short-wavelength lasers are, owing to the decreasing diffraction limit, focusable to small, usually micron- or submicron-sized, spots. Such spots can, however, exhibit complex spatial structures due to intrinsic wavefront properties and/or distortions induced along the beamline. Modeling and numerical analysis of such non-Gaussian beams is not an easy task since complex numerical wavefront propagation algorithms are required [15]; such a topic is beyond the scope of this paper. However, for the sake of illustration, we may study artificially constructed non-Gaussian beams as an approach to real situations.

Table 1. Parameters of the interfering Gaussian modes

Mode parameters		1st Gaussian mode	2nd Gaussian mode
Wavelength	λ [nm]	13.5	13.5
Electric field intensity	E [a.u.]	7	4
Centroid position	x_c [μm]	0	0.7
	y_c [μm]	0	1.1
Waist position	z_{cx} [μm]	−100	400
	z_{cy} [μm]	100	600
Rayleigh range	z_{0x} [μm]	300	200
	z_{0y} [μm]	150	300

To model such a non-Gaussian beam, two astigmatic mutually fully coherent diffraction limited and collinearly polarized Gaussian modes (TEM_{00}) were superposed. The parameters of the interfering modes are listed in Table 1. The electric field amplitudes E_1 and E_2 are, without loss of generality, given in arbitrary units. As the modes are simple astigmatic, each aligned with the x, y axes, two Rayleigh ranges and two longitudinal waist positions must be introduced for the respective x and y electric field components. The waists' locations of the modes are longitudinally separated by 500 μm. By analogy to a real situation, the first mode may represent an image of a laser source and the second mode (focalized further from the focus) may stand for an image of some obstacle (aperture, wire, mirror edge, etc.) inserted into the beam. The second mode is displaced off the optical axis by ~1.3 μm which is leading to an asymmetric beam shape shown in Fig. 2(a). Both particular modes $E_1(\mathbf{r})$ and $E_2(\mathbf{r})$ represent a solution of the paraxial Helmholtz equation (PHE) [16], hence, modal superposition $E_1(\mathbf{r}) + E_2(\mathbf{r})$ is to be regarded as a valid PHE solution as well.

The simulated beam, i.e., the fluence profile $F(\mathbf{r}) \sim |E_1(\mathbf{r}) + E_2(\mathbf{r})|^2$ at a z-position close to the focus, is shown in Fig. 2(a). Even though only two modes were involved in the simulation, we may observe a relatively complicated evolution of the beam profile when scanning through the focus along the z-axis (from z = −800 μm to z = 1200 μm) as shown in Media 1. In Fig. 2(b), four distinct caustic curves, corresponding to four different spot size definitions, are plotted. Here, the black circles stand for the effective caustic curve $A_{eff}(z)$; according to the theory, it is to be regarded as a baseline for the other caustic curves. Blue open circles and dark gray asterisks represent calculated spot areas at 1/e and 1/2 of the maximum fluence $F_0(z)$, respectively. All three curves $A_{eff}(z)$, $S_{1/e}(z)$, and $S_{1/2}(z)$ exhibit two local minima corresponding to the tightest focalization of the two participating modes, whereas the caustic curve $S_{RMS}(z) = \pi\sigma_x(z)\sigma_y(z)$ (red bars), calculated according to the ISO standards for simple astigmatic beams [6–8], tends to a nearly parabolic shape with one local minimum. The squared radii $\sigma_x^2(z)$ and $\sigma_y^2(z)$ are both represented by perfect parabolic functions of z which

#136453 - $15.00 USD Received 14 Oct 2010; revised 3 Dec 2010; accepted 6 Dec 2010; published 17 Dec 2010

are, owing to the astigmatism, mutually slightly separated. This, in fact, confirms Siegman's statement [17] that these parabolic caustic curves should hold for an arbitrary beam (Gaussian or non-Gaussian) if and only if the radii are measured in terms of 2nd order statistical moments. The difference between the caustic curves in Fig. 2(b) is apparent and must be taken in account in order to avoid underestimation or overestimation of the real peak fluence $F_0(z)$.

The utilization adequacy of each particular spot size definition should be premeditated first to meet the requirements of the experiment. The effective area provides the best results for the peak fluence, whereas the spot size related to 2nd order statistical moments (especially 4σ and/or d_{86} definition) is the best approach to evaluate the averaged fluence and the beam propagation factor (M-squared) [6–8,17]. Finally, we should point out that for an ideal astigmatic single mode Gaussian beam all caustic curves overlap if rescaled by multiplication factors: $A_{eff}(z) = 2S_{RMS}(z) = S_{1/e}(z) = S_{1/2}(z)/\ln(2)$. In case of a non-Gaussian beam, however, no deterministic relation between these quantities is known.

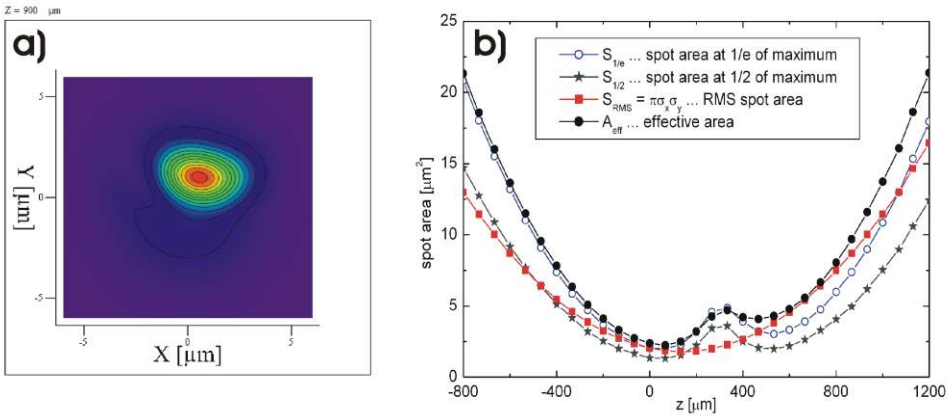

Fig. 2. A simulation of a non-Gaussian beam consisting of two interacting Gaussian modes propagating alongside the optical z-axis. (a) An asymmetric two-dimensional irradiance profile at one of the simulated positions z = 900 µm (Media 1). (b) Four characteristic caustic curves corresponding to different spot area definitions.

3. Experimental methods

In this section, we focus on experimental methods to measure the transverse beam profile and the spot size, based on ablation imprints in various materials. We first recall methods published earlier in [2,18] dealing with ablation imprints in solid state materials. Next, we apply all above formalism to PMMA beam profile measurements and, finally, we develop a new method to measure the effective area.

3.1 Liu's analysis

One of the methods, which was used to characterize the focal spot area (spot size) of soft X-ray laser beams, was first proposed by Liu [18]. Nevertheless, this method is restricted to Gaussian beams only. In brief, plotting the ablation imprint areas, created by single laser shots in a solid material, in relation to the pulse energy logarithm should provide a linear sequence to be fitted by a line. The beam spot area is then given by the slope of the linear fit and the ablation threshold pulse energy (E_{th}) is to be determined by linear extrapolation to zero imprint area, i.e, no surface damage.

In case of a non-Gaussian beam, however, the dependence of the crater (imprint) pedestal areas on the pulse energy logarithm may become non-linear as illustrated in Fig. 3(b). Such a non-linear behavior could be incorrectly attributed to material properties and might introduce severe inaccuracies into the results leading to an undesirable misinterpretation of the laser-matter interaction experiment. Figure 3(a) is depicting one of the non-Gaussian ablative

#136453 - $15.00 USD Received 14 Oct 2010; revised 3 Dec 2010; accepted 6 Dec 2010; published 17 Dec 2010

imprints in PMMA (fabricated by Silson, UK) created by FLASH tuned at 13.5 nm. In Fig. 3(b), two linear fits have been performed both showing different and ambiguous results. The slope at the low pulse energy end of the data is much less than the slope at the high pulse energy end. Basically, this indicates that the incident beam was surrounded by wings being responsible for the beam profile pedestal broadening and, consequently, for the non-linear nature of the Liu's plot.

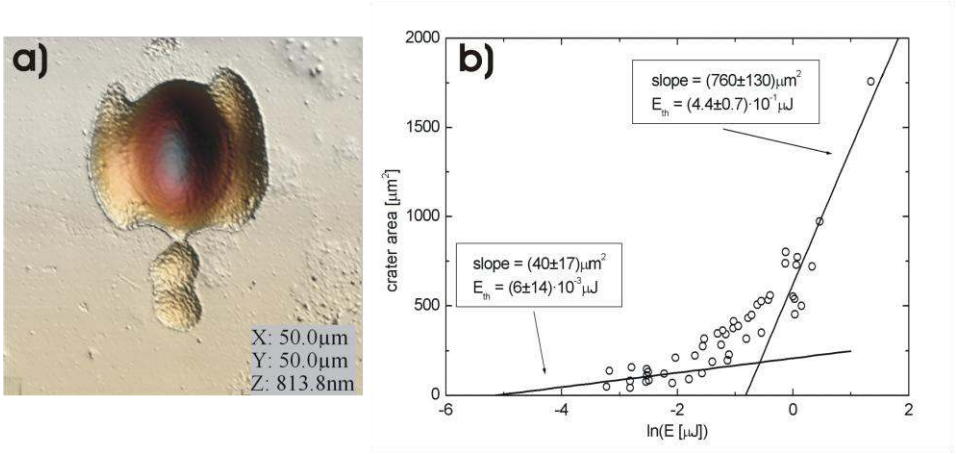

Fig. 3. (a) A non-Gaussian ablative imprint in PMMA showing a presence of wings broadening the beam profile. (b) A non-linearity in the Liu's plot preventing determination of both the ablation threshold (E_{th}) and the beam spot size (slope).

3.2 Transverse beam profile reconstruction

The beam profile shown in Fig. 1 was reconstructed using the PMMA ablative imprint method reported in [2]. This method allows the visualization of the transverse fluence distribution F(x,y) at a chosen z-position down to the limiting threshold fluence. Let us omit the z-dependence in order to abbreviate the following equations.

Primarily, the method of the transverse beam profile F(x,y) retrieval is based on the Lambert-Beer law of the radiation attenuation in a solid state material. Furthermore, it needs to be assumed that the attenuation length of the material is much shorter than the Rayleigh range of the beam ($l_{at} << z_0$); this, in other words, means a negligible variation of the beam profile with the depth coordinate in the crater interior. The complex refractive index of PMMA approaches to (1 + 0i) for the short-wavelength radiation [19]; the surface reflectivity is, thereby, negligible under normal incidence conditions. Accordingly, the fluence inside the material is below the PMMA surface distributed as:

$$F_{PMMA}(x,y,d) = F(x,y)\exp(-d/l_{at}). \quad (3)$$

Here, d denotes the longitudinal coordinate originating at the sample surface being located at position z. Due to the fact that the laser ablation occurs solely above some ablation threshold F_{th}, we obtain a boundary condition (implicit equation) for the ablated crater surface morphology d(x,y):

$$F_{PMMA}(x,y,d(x,y)) = F_{th} = F(x,y)\exp(-d(x,y)/l_{at}). \quad (4)$$

Consequently, the transverse beam profile F(x,y) at the target plane is to be retrieved directly from the measured spatial morphology d(x,y) of the beam imprint in PMMA analyzed by AFM (Atomic Force Microscope), as:

$$F(x,y) = F_{th}\exp(d(x,y)/l_{at}). \quad (5)$$

#136453 - $15.00 USD Received 14 Oct 2010; revised 3 Dec 2010; accepted 6 Dec 2010; published 17 Dec 2010

Our experimental measurements performed at FLASH tuned at 13.5 nm have shown that the PMMA attenuation length and the non-thermal ablation threshold are l_{at} = 175 nm and F_{th}~30 mJ/cm^2, respectively. The peak-to-threshold fluence ratio

$$p = F_0 / F_{th}, \tag{6}$$

determined from the maximum of the reconstructed profile in Fig. 1, was p~100.
It confirms that the major part of the beam profile was visualized. Nevertheless, the feasibility of the reconstruction has an upper limit given by thermal ablation threshold of PMMA (~300F_{th} at 13.5 nm) which should not be exceeded by the peak fluence F_0. Non-thermal (p = 1) and thermal (p~300) ablation thresholds define the dynamic range of PMMA for reliable beam profile analysis at 13.5 nm.

The transverse beam profile reconstruction utilizing PMMA ablative imprints, has been used successfully in the soft X-ray spectral domain at 21.7 nm [2] and 13.5 nm [5]. However, going to shorter wavelengths (higher photon energies) brings difficulties in the sense of roughening the ablated PMMA surface. The effect of the surface roughening is a direct consequence of the increasing attenuation length when the X-ray photon energy approaches the carbon K-edge at ~285 eV [19]. Therefore, new generally high-Z materials need to be used in order to extend the available spectral range deeper to soft X-ray domain.

3.3 Effective area measurement (F-scan)

It follows from Eq. (2b) that the effective area is to be calculated directly as a numerical integral of the transverse beam profile. For the sake of simplicity, let us focus again on a certain (x,y) plane at a chosen z-position. Applying the beam profile reconstruction method to a PMMA ablative imprint as reported in [2], we obtain a non-normalized beam profile $f(x,y) \propto \exp(d(x,y)/l_{at})$ which has to be first modified before the numerical integration is done. Primarily, the truncated part below the PMMA non-thermal ablation threshold, where d(x,y) = 0, has to be excluded from the integration by setting to zero, otherwise a non-physical value would be added to the result. Next, the whole profile has to be normalized by the factor $p = \exp(d_{max}/l_{at}) = F_0/F_{th}$, where d_{max} denotes the maximum crater depth, to obey the condition that $f(x,y) \leq 1$ throughout the (x,y) plane. Such a normalization could be, however, a source of an inaccuracy for noisy beams; therefore, data smoothing needs to be applied to the crater or beam profile to prevent an underestimation of the result. The truncation effect, associated with the threshold-like behavior of PMMA, is responsible for a systematic error in the effective area estimation scaling approximately as 1/p; thus, the best results should be obtained for the peak-to-threshold fluence ratio as high as possible, whilst not exceeding the thermal ablation threshold.

The normalized reconstructed beam profile provides information about the cross-section area at any level of fluence down to the ablation threshold level 1/p. Figure 4 shows the dependence f(S) of the normalized fluence level f on the cross-section area S as determined from the beam profile plotted in Fig. 1. Furthermore, an exponential curve corresponding to an ideal Gaussian beam, having the same cross-section area at 1/e of maximum as the measured profile, is introduced. Apart from a small contribution of the beam profile below the non-thermal ablation threshold (truncated part), the effective area is represented by the area below this curve and is to be expressed as the one-dimensional integral of the following form:

$$A_{eff} = \int_0^{S_{MAX}} f(S)\,dS, \tag{7}$$

where the integration limit S_{MAX} denotes the crater pedestal area enclosed by the threshold contour. Let us conclude the part concerning the effective area measurement utilizing ablative imprints in PMMA with a brief summary of steps to be followed:

1. Record an ablative imprint of the beam at the desired z-position in PMMA.
2. Perform an AFM measurement of the imprint.

#136453 - $15.00 USD Received 14 Oct 2010; revised 3 Dec 2010; accepted 6 Dec 2010; published 17 Dec 2010

3. Smooth the crater profile if necessary.

4. Reconstruct the beam profile using formula: $f(x,y) \propto \exp(d(x,y)/l_{at})$. If the attenuation length l_{at} is not known, use the tabulated value [19].

5. Set the truncated part, where $d(x,y) = 0$, to zero.

6. Calculate the peak-to-threshold ratio as $p = \exp(d_{max}/l_{at})$ and estimate the truncation error (~1/p).

7. Normalize the beam profile: $f(x,y) = p^{-1}\exp(d(x,y)/l_{at})$.

8. Calculate the effective area using Eq. (2b).

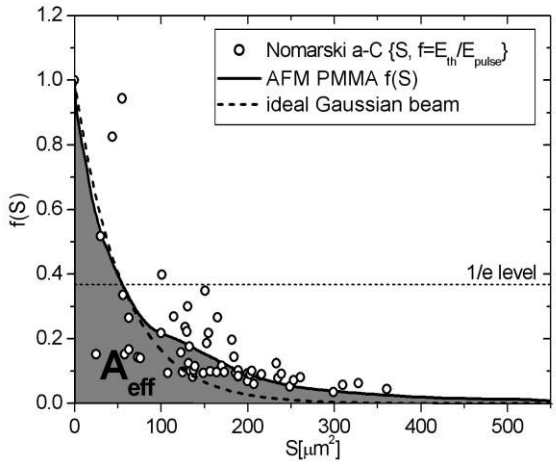

Fig. 4. Normalized fluence level in relation to the corresponding cross-section area of the reconstructed beam profile (black solid line), ideal Gaussian beam (black dashed line), and the dependence of the threshold-to-peak fluence ratio $f = 1/p = E_{th}/E_{pulse}$ on the ablated crater area S in a-C (open circles).

In fact, the definition of the effective area given by Eq. (7) opens up another way of the beam spot size measurement. Any solid state material with a sharp irradiance-independent single-shot ablation threshold F_{th} visualizes the beam contour at level $f = 1/p = F_{th}/F_0 = E_{th}/E_{pulse}$ since only the part of the beam profile above the threshold contributes to the ablation. Such a measurement was performed using 890 nm thick layer of amorphous carbon (a-C) on a silicon substrate (fabricated by GKSS, Germany). Measurements using PMMA (see Fig. 1) and a-C were conducted at the same time under the same beam conditions to get a comparison between these two different materials. Several imprints were created by FLASH focused on the surface of a-C at various pulse energies E_{pulse} acquired by a gas monitor detector (GMD) [20]. The ablated crater areas were *ex situ* determined using the Nomarski microscope; Fig. 5. The areas were plotted as a function of the measured pulse energy logarithm, and the threshold pulse energy E_{th}~0.36 μJ was evaluated by a linear extrapolation of such a plot to zero ($S = 0$ μm^2) where no ablation occurs. Usually, the low energy part of the data is to be involved into the extrapolation since the high energy part may be affected by nonlinearities related to the non-Gaussian nature of the beam. Open circles in Fig. 4 show the dependence of the threshold-to-peak fluence ratio $f = 1/p = E_{th}/E_{pulse}$ on the corresponding crater pedestal area S. Such a plot is, in fact, representing an F-scan (fluence scan) through the beam profile. Although not measured, the data point $f(0) = 1$ may be artificially but legally added to the measured data set. By analogy with Eq. (2b), the effective area is to be calculated as a numerical integral of the data set applying, for example,

#136453 - $15.00 USD Received 14 Oct 2010; revised 3 Dec 2010; accepted 6 Dec 2010; published 17 Dec 2010

the trapezoidal rule of integration (summation). The upper limit of the summation is given by the maximum observed crater area. The measurements carried out with these two materials are in a good agreement even though an increased variance in a-C measurement is indicating relatively high shot-to-shot fluctuations of the beam profile. The effective areas were evaluated and the error bars estimated as $A_{eff,\,PMMA} = (71 \pm 5)\ \mu m^2$ and $A_{eff,\,aC} = (70 \pm 10)\ \mu m^2$ for PMMA and amorphous carbon, respectively.

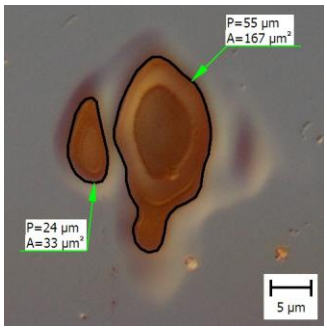

Fig. 5. Nomarski micrograph of an imprint of the focused FLASH beam in a-C; the ablated area is highlighted and measured (P stands for the contour circumference and A for its area).

Using the F-scan, i.e., visualization of the beam contours at various fluence levels, has certain advantages against the direct beam profile reconstruction. First, any time-consuming AFM measurement is not needed. Second, the contour measurement is less sensitive to high-irradiance thermal and other transverse effects which occur mainly in the crater interior. Third, this method might be extended to other wavelength regions and used for different pulse durations when an appropriate material is chosen.

4. Conclusions

In conclusion, a new technique for an analysis of focused non-Gaussian (i.e., distorted, fragmented, non-homogeneous) laser beams has been reported. A general beam parameter called effective area has been utilized to characterize the real beam spot area. The effective area analysis has been employed in the beam profile characterization using an ablative imprint of FLASH beam in PMMA. Finally, it has been found that the F-scan method, applied to ablative imprints in amorphous carbon, provides comparable results to the PMMA beam profile reconstruction.

Acknowledgments

This work was partially funded by the Czech Ministry of Education (Projects LC510, LC528, ME10046, and LA08024), Czech Science Foundation (GD202/08/H057 and P208/10/2302) and by Academy of Sciences of the Czech Republic (Grants AV0Z10100523, IAAX00100903, and KAN300100702). The support for access to FLASH by DESY and by the European Community under contract RII3-CT-2004-506008 (IA-SFS) is gratefully acknowledged. We finally thank the whole FLASH team at DESY for supporting this work.

#136453 - $15.00 USD Received 14 Oct 2010; revised 3 Dec 2010; accepted 6 Dec 2010; published 17 Dec 2010